Available online at www.sciencedirect.com
SCIENCE DIRECT
Remote Sensing of Environment 101 (2006) 13 – 24
Remote Sensing of Environment
www.elsevier.com/locate/rse

Estimating chlorophyll *a* concentrations from remote-sensing reflectance in optically shallow waters

Jennifer Patch Cannizzaro *, Kendall L. Carder

University of South Florida, St. Petersburg, FL, United States

Received 11 August 2005; received in revised form 29 November 2005; accepted 1 December 2005

Abstract

A multi-spectral classification and quantification technique is developed for estimating chlorophyll *a* concentrations, Chl, in shallow oceanic waters where light reflected by the bottom can contribute significantly to the above-water remote-sensing reflectance spectra, $R_{rs}(\lambda)$. Classification criteria for determining bottom reflectance contributions for shipboard $R_{rs}(\lambda)$ data from the west Florida shelf and Bahamian waters (1998–2001; $n=451$) were established using the relationship between $R_{rs}(412)/R_{rs}(670)$ and the spectral curvature about 555 nm, $[R_{rs}(412)*R_{rs}(670)]/R_{rs}(555)^2$. Chlorophyll concentrations for data classified as "optically deep" and "optically shallow" were derived separately using best-fit cubic polynomial functions developed from the band-ratios $R_{rs}(490)/R_{rs}(555)$ and $R_{rs}(412)/R_{rs}(670)$, respectively. Concentrations for transitional data were calculated from weighted averages of the two derived values. The root-mean-square error ($RMSE_{log10}$) calculated for the entire data set using the new technique was 14% lower than the lowest error derived using the best individual band-ratio. The standard blue-to-green, band-ratio algorithm yields a 26% higher $RMSE_{log10}$ than that calculated using the new method. This study demonstrates the potential of quantifying chlorophyll *a* concentrations more accurately from multi-spectral satellite ocean color data in oceanic regions containing optically shallow waters.

Keywords: Remote sensing; Chlorophyll; Algorithm; Shallow; Empirical; Ocean color

1. Introduction

The quantity and spectral quality of light reflected by the ocean's surface or water-leaving radiance, $L_w(\lambda)$, are controlled by the inherent optical properties (IOP) of the water column (absorption, $a(\lambda)$, and backscattering, $b_b(\lambda)$), downwelling irradiance, $E_d(\lambda)$, and the angular distribution of light within the ocean (Gordon et al., 1988). For optically shallow waters, radiance reflected by the bottom also contributes to $L_w(\lambda)$ and can vary with bottom depth, H, and bottom albedo, $\rho(\lambda)$ (Carder et al., 1993; Lee et al., 1998a, 1998b, 1999; Lyzenga, 1978; Maritorena et al., 1994; Spitzer & Dirks, 1987).

Most empirical ocean color algorithms for deriving chlorophyll *a* concentrations, Chl, have been developed primarily for optically deep waters where bottom reflectance is negligible. Such algorithms strongly depend upon correlations between Chl and spectral blue-to-green ratios of $L_w(\lambda)$ or remote-sensing reflectance, $R_{rs}(\lambda)$, where $R_{rs}(\lambda)$ is equal to the ratio of water-leaving radiance to downwelling irradiance. The blue waveband is traditionally located near the phytoplankton absorption peak (~440 nm) where chlorophyll *a* absorbs maximally. The green or "reference" waveband is typically located in a region of minimal phytoplankton absorption (~550 to 555 nm). For Coastal Zone Color Scanner (CZCS) data (1978–1986), chlorophyll concentrations were estimated using ratios of $L_w(443)/L_w(550)$ (Gordon et al., 1983). Although this algorithm was validated with field data collected from fewer than 60 stations, it successfully provided accurate pigment concentrations to ±40% accuracy in optically deep waters where phytoplankton dominated the optical properties.

The blue waveband in blue-to-green, band-ratio algorithms has also been red-shifted from ~440 nm to 490 and 510 nm to minimize interference due to colored dissolved organic matter (CDOM) absorption that absorbs blue light strongly and signal-to-noise errors that occur with increasing chlorophyll and

* Corresponding author. Tel.: +1 727 553 3954.
E-mail address: jpatch@marine.usf.edu (J.P. Cannizzaro).

0034-4257/$ - see front matter © 2006 Elsevier Inc. All rights reserved.
doi:10.1016/j.rse.2005.12.002

CDOM concentrations (O'Reilly et al., 1998, 2000). Although, phytoplankton absorption at 490 and 510 nm is dominated by accessory pigments, chlorophyll *a* concentrations can be derived accurately from these band-ratios because accessory pigment and chlorophyll concentrations are highly correlated (Trees et al., 2000). Algorithms for the Sea-viewing Wide Field-of-View Sensor (SeaWiFS) (OC4) and Moderate Resolution Imaging Spectroradiometer (MODIS) (OC3m) currently employ a maximum band-ratio approach using all three of these or similar band-ratios with a fourth-order polynomial function (O'Reilly et al., 1998, 2000).

The "reference" waveband in most empirical reflectance-ratio chlorophyll algorithms is located inside the spectral transparency window (~450 to 600 nm) where light entering the ocean penetrates the deepest. Bottom reflectance at these wavelengths can significantly increase reflectance values causing chlorophyll concentrations estimated using algorithms developed for optically deep data to be overestimated (D'Sa et al., 2002; Lee et al., 2001). Techniques for partitioning $R_{rs}(\lambda)$ into water column and bottom reflectance spectra in order to remove bottom contributions, therefore, are highly desirable. Numerous such inversion techniques have been developed (Lee et al., 1998a, 1998b, 1999; Louchard et al., 2003; Mobley et al., 2005; Sandidge & Holyer, 1998), but most are designed to perform optimally with hyperspectral $R_{rs}(\lambda)$ data.

Remote-sensing reflectance spectra have been successfully partitioned analytically using a bio-optical model parameterized with measured water column optical properties, bottom depths, and bottom albedos (Gould & Arnone, 1997). In the absence of measured input parameters, an optimization technique that simultaneously derives $a(\lambda)$, $b_b(\lambda)$, H and $\rho(\lambda)$ from $R_{rs}(\lambda)$ was developed by inverting a semi-analytical reflectance model and optimizing the unknown parameters (Lee et al., 1998a, 1998b, 1999). Look-up tables (LUT) (Louchard et al., 2003; Mobley et al., 2005) and neural network (Sandidge & Holyer, 1998) approaches are also used to extract water column optical properties, bottom depths and bottom albedos from hyperspectral $R_{rs}(\lambda)$ data.

While ocean color sensors mounted on ships, moorings, and aircrafts can afford to be hyperspectral, satellite ocean color sensors (e.g. SeaWiFS and MODIS) remain multispectral due to data storage limitations. Satellite ocean color sensors provide high frequency synoptic information over large areas, thereby offering an optimal platform for long-term monitoring of global ocean color and its derived products (e.g. $a(\lambda)$, $b_b(\lambda)$, and Chl). Inversion techniques for partitioning remote-sensing reflectance spectra into water column and bottom reflectance components perform less accurately with multi-band $R_{rs}(\lambda)$ data and can be computationally expensive when applied to entire scenes (Hu et al., 1998; Lee & Carder, 2002).

In this study, shipboard hyperspectral $R_{rs}(\lambda)$ data collected from the west Florida shelf (WFS) and Bahamian waters are partitioned into water column and bottom reflectance spectra using the Lee et al. (1999) optimization technique. The percentage contribution bottom reflectance makes to $R_{rs}(555)$ could then be calculated. These values are considered while examining the performance of both standard and alternative empirical band-ratio algorithms for estimating chlorophyll concentrations from $R_{rs}(\lambda)$. A technique requiring $R_{rs}(\lambda)$ data at only four wavebands (412, 490, 555 and 670 nm) that (1) classifies data as optically deep or optically shallow and (2) quantifies chlorophyll concentrations more accurately in regions containing unknown bottom reflectance contributions is developed. When applied to satellite ocean color data, this technique has the potential to improve estimations of chlorophyll concentrations in shallow oceanic waters such as the WFS and near the Bahamas where concentrations are typically overestimated.

2. Data and methods

Shipboard data were collected during 27 research cruises during four major field programs between 1998 and 2001 (Table 1, Fig. 1). The Tongue of the Ocean (TOTO) (1998–2000; $n=86$) and Coastal Benthic Optical Properties (CoBOP) (1998–2000; $n=105$) programs were based in Bahamian waters located in the Tongue of the Ocean and in waters offshore of Lee Stocking Island, respectively. Data from the WFS , Florida Straits, NW and NE Providence Channel and Grand Bahamas Bank were collected during transit for these programs. West Florida shelf data were also collected as part of the Ecology and Oceanography of Harmful Algal Blooms (ECOHAB) (1999–2001; $n=224$) and the

Table 1
Cruise data summary

Program	Cruise	Location	Dates
TOTO	tt0498	Bahamas, Florida Straits, and west Florida shelf	04/01/98–04/07/98
	tt0499		04/12/99–04/19/99
	tt0400		04/23/00–04/30/00
CoBOP	cbp0598	Bahamas, Florida Straits, and west Florida shelf	05/15/98–06/02/98
	cbp0599		05/17/99–06/07/99
	cbp0500		05/13/00–06/01/00
FSLE	FSLE3	West Florida shelf	07/01/00–07/10/00
	FSLE4		11/04/00–11/14/00
	FSLE5		04/18/01–04/26/01
ECOHAB	eh0399	West Florida shelf	03/01/99–03/04/99
	eh0799		07/05/99–07/08/99
	eh0999		09/07/99–09/10/99
	eh1199		11/06/99–11/08/99
	eh0100		01/11/00–01/14/00
	eh0300		03/01/00–03/04/00
	eh0800		08/02/00–08/05/00
	eh1000		10/04/00–10/06/00
	eh1100		11/07/00–11/10/00
	eb0201		02/06/01–02/07/01
	eh0401		04/03/01–04/06/01
	eh0601		06/05/01–06/08/01
	eh0701		06/30/01–07/03/01
	eh0801		08/01/01–08/01/01
	eh0901		08/28/01–08/31/01
	eb0901		08/29/01–08/30/01
	eb1001		10/01/01–10/02/01
	hy1001		10/04/01–10/04/01

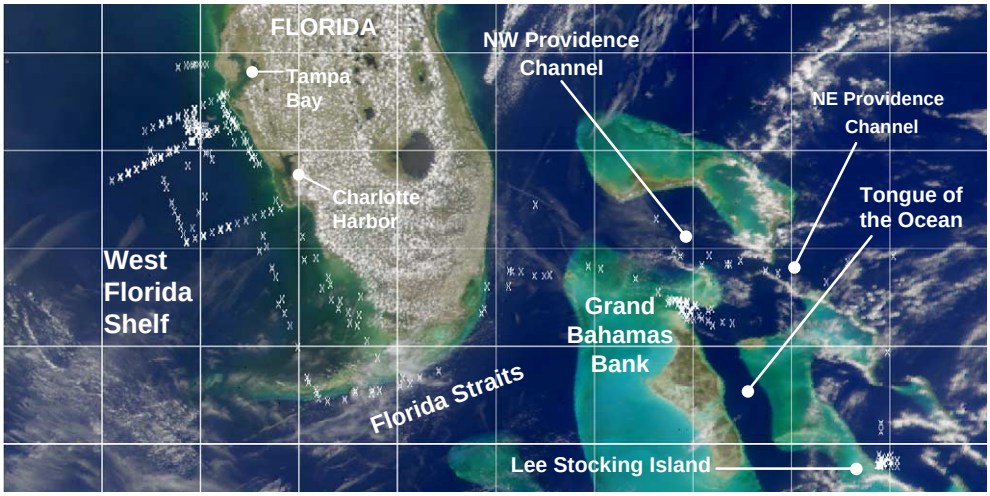

Fig. 1. SeaWiFS quasi-true color image (16 March 2002) of the study area. Station locations (×) for the CoBOP, TOTO, FSLE, and ECOHAB cruises (1998–2001) are shown. Generally, waters that are optically shallow (e.g. Grand Bahama Bank) appear blue–green due to high bottom reflectance contributions while optically deep waters appear dark blue.

Florida Shelf Lagrangian Experiment (FSLE) (2000–2001; $n=50$) programs.

Absorption and backscattering measurements were made to validate model results obtained using the optimization technique (Lee et al., 1999). $R_{rs}(\lambda)$ and Chl data were used to examine the performance of various empirical band-ratio chlorophyll algorithms.

2.1. Discrete surface samples

Surface water samples were collected using Niskin bottles or buckets and were filtered immediately. Absorption spectra due to particulates, $a_p(\lambda)$, and detritus, $a_d(\lambda)$, were determined using the quantitative filter technique (Kiefer & SooHoo, 1982; Yentsch, 1962). Measurements were made with a custom-made, 512-channel spectral radiometer (~350 to 850 nm, ~2.5 nm resolution) (Bissett et al., 1997). Pigments were extracted with hot methanol (Kishino et al., 1985; Roesler et al., 1989) from which chlorophyll *a* concentrations were determined fluorometrically (Holm-Hansen & Riemann, 1978). Optical pathlength elongation was corrected using an average of two previously reported beta factors (Bricaud & Stramski, 1990; Nelson & Robertson, 1993). Phytoplankton absorption spectra, $a_{ph}(\lambda)$, were then calculated as the difference between $a_p(\lambda)$ and $a_d(\lambda)$.

CDOM absorption spectra, $a_{CDOM}(\lambda)$, were measured on 0.2 μm filtered surface seawater samples using a dual-beam spectrophotometer (Perkin-Elmer® Lambda 18). Data were processed using methods previously described by Mueller and Fargion (2002).

2.2. Underway surface samples

Underway measurements of backscattering were obtained during ECOHAB cruises (2000–2001) using a Hydroscat-2 (HOBI Labs®). Measurement, calibration, and data processing information for this instrument have been described previously (Maffione & Dana, 1997). A spectral power function was fit to measured backscattering values at 488 and 676 nm in order to obtain the backscattering coefficient at 550 nm. Particulate backscattering at 550 nm, $b_{bp}(550)$, was calculated from total backscattering by subtracting the backscattering due to pure water (Morel, 1974).

2.3. Remote-sensing reflectance

Remote-sensing reflectance spectra, $R_{rs}(\lambda)$, were measured as

$$R_{rs}(\lambda)_{meas} = \frac{L_w(\lambda)}{E_d(\lambda)}. \quad (1)$$

$L_w(\lambda)$ and $E_d(\lambda)$ were calculated from above-water measurements of upwelling radiance, sky radiance, and the radiance reflected from a Lambertian "graycard" reflector (Spectralon®; ~10%) using methods described previously by Lee et al. (1997). All measurements were made using a custom-made, 512-channel spectral radiometer (~350 to 850 nm; ~2.5 nm resolution).

3. Optimization technique

In order to examine how bottom reflectance influences empirical band-ratio chlorophyll algorithms, the percentage contribution bottom reflectance makes to the remote-sensing reflectance at 555 nm, %bt_555, was determined. Shipboard hyperspectral $R_{rs}(\lambda)$ data were inverted using a semi-analytical reflectance model with separate terms for water column and bottom reflectance. Values for $a_{ph}(440)$, $a_{CDOM}(440)$, $b_{bp}(550)$, $\rho(550)$, and H were solved simultaneously using a predictor–corrector optimization technique (Lee et al., 1999). Retrieved values were then fed back into the model to calculate %bt_555. The $R_{rs}(\lambda)$ model and optimization technique are described briefly below.

3.1. Semi-analytic model

Remote-sensing reflectance spectra below the air–sea interface, $r_{rs}(\lambda)$, is related to that above the sea surface as (Lee et al., 1999)

$$R_{rs}(\lambda)_{mod.} \frac{0.5r_{rs}(\lambda)}{1-1.5r_{rs}(\lambda)} \quad (2)$$

for a nadir-viewing sensor. This expression accounts for the water-to-air divergence factor and internal reflection of the water–air interface (Morel & Gentili, 1993). For brevity, wavelength, λ, shall be omitted in the following equations unless it is necessary to include for clarity.

The subsurface remote-sensing reflectance can be separated into water column and bottom reflectance components as (Lee et al., 1999)

$$r_{rs} \approx r_{rs}^{dp}\left[1-\exp\left(-\left(\frac{1}{1.2}+\frac{D_u^C}{0.92}\right)\kappa H\right)\right] + \frac{1}{\pi}\rho\exp\left(-\left(\frac{1}{1.2}+\frac{D_u^B}{0.92}\right)\kappa H\right) \quad (3)$$

where r_{rs}^{dp} is the subsurface remote-sensing reflectance for optically deep waters, D_u^C is the optical path elongation factor for the water column, D_u^B is the optical path elongation factor for the bottom, and κ is equal to the sum of the absorption and backscattering coefficients.

Subsurface remote-sensing reflectance for optically deep waters is (Lee et al., 2004)

$$r_{rs}^{dp} = g_w\frac{b_{bw}}{a+b_b} + g_p\frac{b_{bp}}{a+b_b} \quad (4)$$

where g_w and g_p are known model-derived parameters for molecular and particle scattering, respectively. Separate terms for particles and molecules are required because the angular distribution for molecular backscattering due to water, $b_{bw}(\lambda)$, differs from that of particulate backscattering due to water.

Optical path elongation factors for the water column and bottom are (Lee et al., 1999)

$$D_u^C \approx 1.03(1+2.4u)^{0.5} \text{ and } D_u^B \approx 1.04(1+5.4u)^{0.5}, \quad (5)$$

respectively, where

$$u = \frac{b_b}{a+b_b}. \quad (6)$$

Absorption and backscattering spectra are decomposed as

$$a = a_w + a_{ph} + a_{CDOM} \quad (7)$$

and

$$b_b = b_{bw} + b_{bp} \quad (8)$$

where absorption due to water, $a_w(\lambda)$, and backscattering due to water are constant and well known (Morel, 1974; Pope & Fry, 1997).

Terms for chlorophyll and CDOM fluorescence and water Raman scattering are not included in this model. The water column is assumed to be homogeneous and the bottom a Lambertian reflector.

3.2. Model parameterization

Combining Eqs. (2)–(8) provides a model for deriving $a_{ph}(\lambda)$, $a_{CDOM}(\lambda)$, $b_{bp}(\lambda)$, $\rho(\lambda)$ and H from $R_{rs}(\lambda)$. These terms are parameterized below in order to reduce the number of unknowns.

Phytoplankton absorption spectra is modeled from $a_{ph}(440)$ as (Lee, 1994)

$$a_{ph}(\lambda) = a_{ph}(440)\left[A_0(\lambda)+A_1(\lambda)\ln\left(a_{ph}(440)\right)\right] \quad (9)$$

where $A_0(\lambda)$ and $A_1(\lambda)$ are empirically derived constants tuned to the $a_{ph}(\lambda)$ data measured in this study. This function ensures that $a_{ph}(\lambda)$ curvature changes appropriately with $a_{ph}(440)$, taking into consideration the natural variability observed in phytoplankton pigmentation and pigment packaging (Bricaud et al., 1995).

Absorption spectra due to CDOM is modeled from $a_{CDOM}(440)$ as (Lee et al., 1999)

$$a_{CDOM}(\lambda) = a_{CDOM}(440)\exp(-S(\lambda-440)) \quad (10)$$

where S is the spectral slope. Since CDOM and detritus both exhibit exponentially decreasing absorption with increasing wavelength, they cannot be derived independently. Therefore, $a_{CDOM}(\lambda)$ and $a_d(\lambda)$ are combined and an average spectral slope (0.015 nm^{-1}) is used (Carder et al., 1989, 1991).

Particle backscattering spectra is modeled from $b_{bp}(550)$ as

$$b_{bp}(\lambda) = b_{bp}(550)\left(\frac{550}{\lambda}\right)^Y \quad (11)$$

where the reference wavelength 550 nm replaces the 400-nm value originally used by Lee et al. (1999). The spectral shape parameter for backscattering, Y, is estimated using an empirical relationship from measured $R_{rs}(443)$ and $R_{rs}(490)$ data and values are limited to the 0–2.5 range (Lee et al., 1999).

Bottom albedo spectra is expressed as

$$\rho(\lambda) = \rho(550)*\rho_{550\ nm-normalized}(\lambda) \quad (12)$$

where $\rho(550)$ is the bottom albedo coefficient at 550 nm and $\rho_{550\ nm\text{-}normalized}(\lambda)$ is a bottom albedo spectra normalized at 550 nm for sand (Lee et al., 1999).

3.3. Model optimization

Since $R_{rs}(750)$ for turbid coastal waters may not be zero, $R_{rs}^{in}(\lambda)$ is defined as

$$R_{rs}^{in} = R_{rs}^{meas} + \Delta. \quad (13)$$

Values for $a_{ph}(440)$, $a_{CDOM}(440)$, $b_{bp}(550)$, $\rho(550)$, H and Δ are then derived iteratively using a predictor–corrector optimization scheme until difference between $R_{rs}(\lambda)_{in}$ and $R_{rs}(\lambda)_{mod.}$ are minimized (Lee et al., 1999). Parameter input values provided to the model are independent of field measurements.

4. Results

4.1. In situ chlorophyll a concentrations

In situ surface chlorophyll *a* concentrations ($n=451$) measured during this study span three orders of magnitude and range between 0.026 and 20.6 mg m^{-3} (Fig. 2). The mean value (0.66 mg m^{-3}) is higher than the global average (~0.24 mg m^{-3}) (Gregg & Conkright, 2002) due to the high degree of coastal proximity displayed by this data set. Based on the oceanic provinces defined by Antoine et al. (1996), 18% of the data are oligotrophic with chlorophyll concentrations less than 0.1 mg m^{-3}, 68% are mesotrophic with concentrations between 0.1 and 1.0 mg m^{-3} and 14% are eutrophic with concentrations greater than 1.0 mg m^{-3}.

The CoBOP and TOTO data sets, collected mainly from Bahamian waters, comprise the majority of the oligotrophic data. Chlorophyll concentrations greater than 0.3 mg m^{-3} measured during these field programs were collected during transit to and from the WFS. The FSLE data were collected on the WFS between the 10 and 50 m isobaths and were mostly mesotrophic. The ECOHAB data, collected on the WFS between the 10 and 85 m isobaths, comprise almost half of the total data set and span all three trophic realms with the majority of data being mesotrophic. The eutrophic data for the ECOHAB program were collected from estuarine waters located outside of Tampa Bay or Charlotte Harbor and from harmful algal blooms of an ichthyotoxic dinoflagellate, *Karenia brevis*.

4.2. Optimization

The wide variability in magnitude and spectral shape for remote-sensing reflectance spectra measured during this study (Fig. 3) confirms that a number of diverse environmental

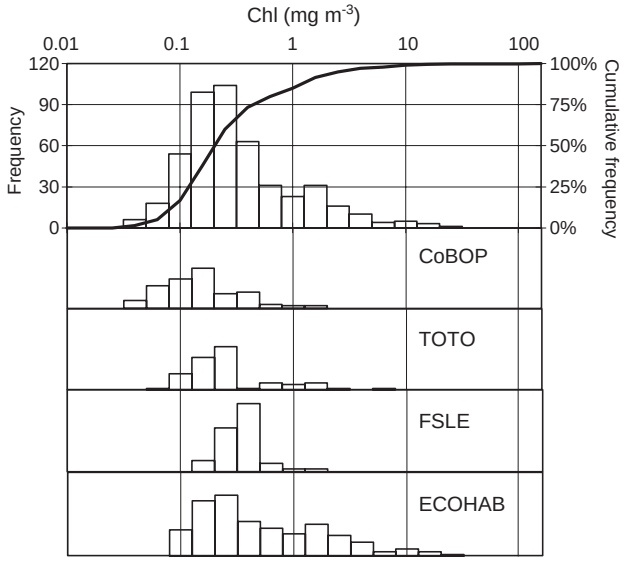

Fig. 2. Frequency distribution for in situ chlorophyll *a* concentrations (mg m^{-3}) for the entire data set ($n=451$) and for each individual field program.

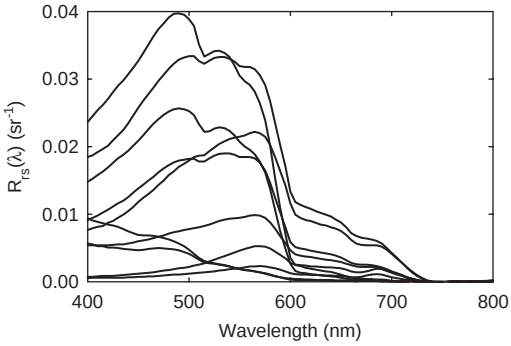

Fig. 3. Examples of measured remote-sensing reflectance spectra (sr^{-1}).

conditions were sampled. Reflectance peaks shift from 400 nm for non-coastal, oligotrophic waters to ~490 nm for highly reflective, optically shallow, mesotrophic waters to ~560 nm for *K. brevis*-dominated, optically deep, eutrophic waters from the WFS.

Measured remote-sensing reflectance spectra were inverted using a semi-analytic reflectance model and values for $a_{ph}(440)$, $a_{CDOM}(440)$, $b_{bp}(550)$, $\rho(550)$, H and Δ were estimated by optimization (Lee et al., 1999). The inversion-derived values were re-inserted into Eqs. (3)–(12) to calculate $r_{rs}(555)$. The contribution that bottom reflectance makes to $r_{rs}(555)$, %bt_555, was then estimated by dividing the second term in Eq. (3) due to bottom reflectance by the total $r_{rs}(555)$.

Confidence in these estimates is determined based on the ability of this technique to accurately retrieve values for $a(440)$, $b_b(550)$, $\rho(550)$ and H. Measured absorption and backscattering values for the various constituents (particles and CDOM) were combined with pure water values (Morel, 1974; Pope & Fry, 1997) to calculate total absorption coefficients at 440 nm and total backscattering coefficients at 550 nm. Measured values were then compared to modeled values derived using the optimization technique (Fig. 4a,b). Root mean square errors determined on log-transformed data ($RMSE_{log10}$) for $a(440)$ and $b_b(550)$ were only 0.105 and 0.101, respectively.

Bottom depths for waters less than 25 m with bottom reflectance contributions at 555 nm greater than 25 and 50% were also retrieved accurately with root mean square errors calculated on non-log-transformed data equal to 0.18 and 0.14, respectively (Fig. 4c). Since $\rho(550)$ was not measured during this study, the retrieval accuracy for this parameter could not be measured. The range of modeled $\rho(550)$ values (0–0.5) observed, however, is within the range of measured and modeled values reported previously (Decho et al., 2003; Lee et al., 2001; Louchard et al., 2003; Werdell & Roesler, 2003).

The majority of $R_{rs}(\lambda)$ data (78%) exhibits bottom reflectance contributions at 555 nm less than 25% and is considered "optically deep" in this study. Model results indicate that 11%, 6% and 5% of the $R_{rs}(\lambda)$ data exhibit %bt_555 values 25–50%, 50–75%, and greater than 75%, respectively. In this study, these data are all considered "optically shallow". Data with %bt_555 values greater than 75% were collected from the Grand Bahamas Bank. Chlorophyll concentrations for these data were ~0.1 to 0.2 mg m^{-3},

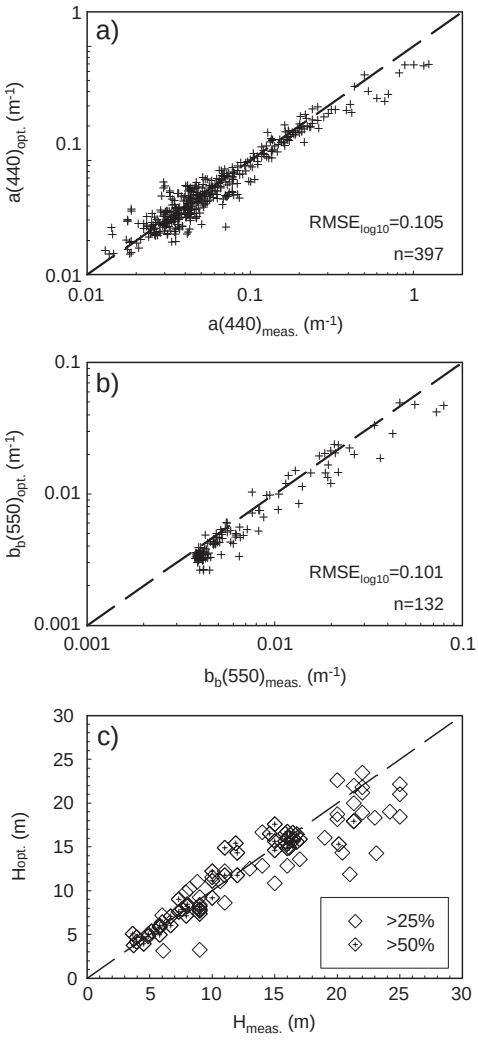

Fig. 4. Measured versus modeled (a) total absorption coefficients at 440 nm (m^{-1}), (b) total backscattering coefficients at 550 nm (m^{-1}), and (c) bottom depths (m). Modeled values were derived from field $R_{rs}(\lambda)$ data using the Lee et al. (1999) optimization technique. Bottom depths are sorted by the percent contribution bottom reflectance makes to $R_{rs}(555)$ into two groups: >25% (diamonds), >50% (diamonds with crosses). One-to-one lines (dashed) are shown.

bottom depths were 4–10 m, and the bottom was composed of highly reflective ($\rho(550)_{mod.}$ ~0.2 to 0.4) sand.

4.3. Performance of standard empirical algorithms

Relationships between measured chlorophyll concentrations and band-ratios, $R_{rs}(\lambda_1)/R_{rs}(\lambda_2)$, using SeaWiFS wavebands where λ_1 is 412, 443, 490 or 510 nm and λ_2 is 555 nm are shown in Fig. 5. Cubic polynomial regression functions were fit to log-transformed, optically deep data with %bt_555 values less than 25% (Table 2).

Band-ratios where λ_1 is 443 or 490 nm generate lower $RMSE_{log10}$ values compared to ratios where λ_1 is 412 or 510 nm. Increased interference by CDOM absorption at 412 nm and the smaller dynamic range displayed by $R_{rs}(510)/R_{rs}(555)$ values compared to the other band-ratios may explain this observation. Error values for these best-fit cubic polynomial relationships are ~25% lower than errors calculated using modified cubic polynomial functions with similar band-ratios (OC2-type) developed for a large global data set assembled during the SeaWiFS Bio-optical Algorithm Mini-Workshop (SeaBAM) (O'Reilly et al., 1998). The lower errors may be explained by the limited geographical extent displayed by the data in this study compared to the SeaBAM data.

For chlorophyll concentrations less than ~0.2 mg m^{-3}, the best-fit cubic polynomial relationships developed from the optically deep (%bt_555<25%) data overlap the OC2-type functions developed by O'Reilly et al. (1998) (Fig. 5)). For chlorophyll concentrations greater than ~0.2 mg m^{-3}, optically deep reflectance ratios measured in this study are generally lower per unit chlorophyll compared to the OC2-type functions. This most likely is due to elevated CDOM-to-chlorophyll ratios observed on the WFS (Cannizzaro et al., in press).

Applying the best-fit cubic polynomial functions developed from the optically deep data to the entire data set results in significant overestimations in chlorophyll concentrations for optically shallow waters (Fig. 5e–h). Statistical analyses performed on log-transformed data indicate high y-intercepts and low coefficients of determination (r^2) (Table 3). $RMSE_{log10}$ values are ~35% to 45% higher when the functions are applied to the entire data set compared to the optically deep data only.

For chlorophyll concentrations between ~0.1 and 0.5 mg m^{-3} where bottom reflectance contributions at 555 nm are greater than 50%, $R_{rs}(\lambda_1)/R_{rs}(555)$ values are generally lower per unit chlorophyll compared to the optically deep data (Fig. 5). Relationships between Chl and $R_{rs}(\lambda)$ for SeaWiFS wavebands (412, 443, 490, 510, 555, and 670 nm) are compared to cubic polynomial relationships determined for the SeaBAM data (Fig. 6) in order to determine why optically shallow reflectance ratios are relatively low.

Greater than 98% of the SeaBAM $R_{rs}(\lambda)$ data occur within a factor of 2 of the SeaBAM best-fit cubic polynomial functions for $R_{rs}(412)-R_{rs}(555)$ and within a factor of 5 for $R_{rs}(670)$. The increased scatter exhibited by $R_{rs}(670)$ data can be attributed to poor signal-to-noise since pure water absorption at 670 nm is ~7 times higher than at 555 nm (Pope & Fry, 1997).

Optically deep (%bt_555<25%) reflectance values for chlorophyll concentrations less than ~0.2 mg m^{-3} are tightly coupled about the best-fit SeaBAM relationships (Fig. 6) and approach clear water radiance values (Eplee & McClain, 2000). Optically deep reflectance values for chlorophyll concentrations greater than ~0.2 mg m^{-3} exhibit increased scatter and pronounced deviations above the SeaBAM relationships. The highly reflective, chlorophyll-rich (>0.5 mg m^{-3}) data were collected from high-backscattering, WFS coastal waters. The less reflective, chlorophyll-rich data were collected primarily from WFS *K. brevis* blooms that exhibit relatively low backscattering-to-chlorophyll ratios (Cannizzaro et al., in press).

Optically shallow (%bt_555>25%) data with chlorophyll concentrations between ~0.1 and 0.5 mg m^{-3} exhibit increased reflectivity compared to both the optically deep data and the SeaBAM best-fit function (Fig. 6). Deviations

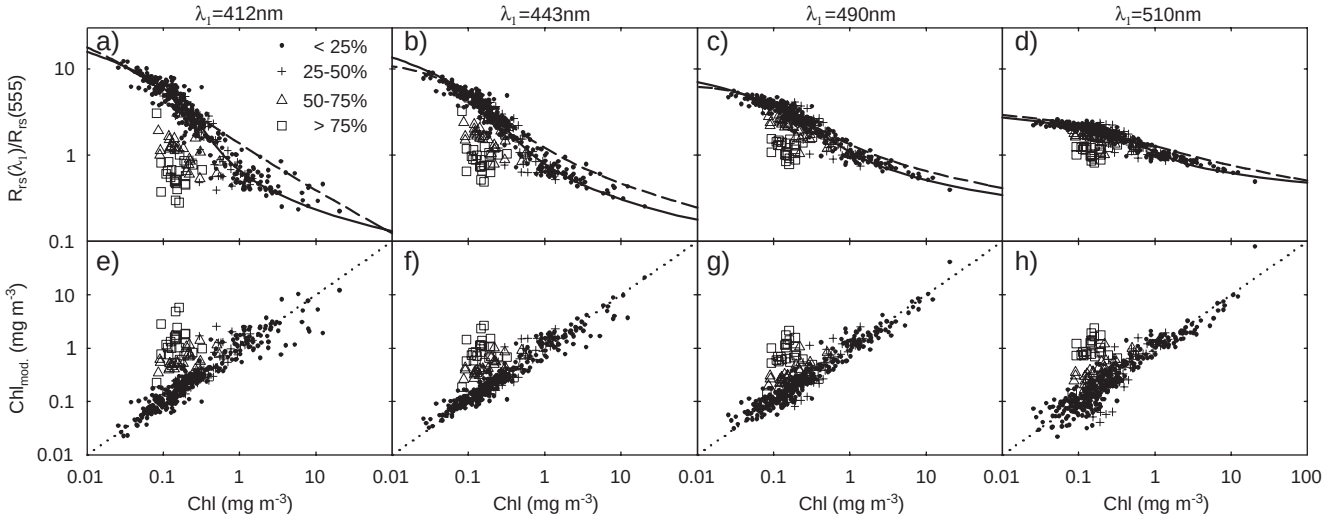

Fig. 5. Relationships between chlorophyll *a* concentrations and $R_{rs}(\lambda_1)/R_{rs}(555)$ (or R) where λ_1 is (a) 412 nm, (b) 443 nm, (c) 490 nm and (d) 510 nm. Data are sorted by the percent contribution bottom reflectance makes to $R_{rs}(555)$ into four groups:<25% (circles), 25–50% (crosses), 50–75% (triangles) and >75% (squares). Cubic polynomial regression functions (solid) were fit to log-transformed optically deep (%bt_555<25%) data: $\log(Chl)=a_0+a_1\log(R)+a_2\log(R)^2+a_3\log(R)^3$. Global OC2-type functions (dashed) developed for the SeaBAM data set are shown for comparison (O'Reilly et al., 1998). The best-fit cubic polynomial functions were applied to the entire data set and (e–h) measured versus modeled chlorophyll *a* concentrations and one-to-one lines (dotted) are shown.

exhibited by these data above the SeaBAM best-fit cubic polynomial functions are lowest for wavebands located outside the spectral transparency window (~450 to 600 nm), $R_{rs}(412)$ and $R_{rs}(670)$, and increase gradually from $R_{rs}(443)$ to $R_{rs}(555)$. Remote-sensing reflectance values at 555 nm within the spectral transparency window are influenced the most by bottom reflectance. Data with bottom reflectance contributions at 555 nm 50–75% and >75% are ~3 and 10 times higher, respectively, than optically deep data with similar chlorophyll concentrations (Fig. 6e).

The tendency for $R_{rs}(555)$ values to increase with increasing bottom reflectance contributions at a faster rate than all the other wavebands explains why optically shallow $R_{rs}(\lambda_1)/R_{rs}(555)$ ratios are relatively low compared to optically deep data. Since chlorophyll concentrations derived empirically in optically shallow waters using traditional blue-to-green band-ratio algorithms developed for optically deep data are over-estimated (Fig. 5), an alternative band-ratio was sought to estimate chlorophyll concentrations more accurately in shallow oceanic waters containing significant bottom reflectance contributions.

The relationship between chlorophyll concentrations and $R_{rs}(670)$ indicates that $R_{rs}(670)$ is less sensitive to increasing bottom reflectance contributions compared to $R_{rs}(555)$ (Fig. 6e,f). Therefore, relationships between chlorophyll concentrations and the same four band-ratios as in Fig. 5 are examined except $\lambda_2=555$ nm is replaced by $\lambda_2=670$ nm (Fig. 7). Cubic polynomial regression functions were fit to the log-transformed, optically deep data with bottom reflectance contributions at 555 nm less than 25% (Table 2).

$RMSE_{log10}$ values were 7–35% higher when applying the best-fit $R_{rs}(\lambda_1)/R_{rs}(670)$ functions to the optically deep data only compared when the best-fit $R_{rs}(\lambda_1)/R_{rs}(555)$ functions were applied (Table 2). Applying these best-fit functions to

Table 2
Cubic polynomial regression coefficients derived empirically between log-transformed chlorophyll *a* concentrations and band-ratios, $R_{rs}(\lambda_1)/R_{rs}(\lambda_2)$ (or R) where λ_1 is 412, 443, 490, and 510 nm and λ_2 is 555 and 670 nm, for data with bottom reflectance contributions at 555 nm less than 25% ($n=350$): $\log(Chl)=a_0+a_1\log(R)+a_2\log(R)^2+a_3\log(R)^3$

Band-ratio	a_0	a_1	a_2	a_3	$RMSE_{log10}$
$R_{rs}(412)/R_{rs}(555)$	−0.2278	−1.0446	0.8278	−0.9923	0.165
$R_{rs}(443)/R_{rs}(555)$	−0.1918	−1.2828	1.4693	−1.8599	0.139
$R_{rs}(490)/R_{rs}(555)$	0.0597	−2.2291	2.6691	−3.4144	0.134
$R_{rs}(510)/R_{rs}(555)$	0.0865	−2.5845	4.1442	−20.5183	0.181
$R_{rs}(412)/R_{rs}(670)$	0.8840	−2.0837	1.3061	−0.3906	0.177
$R_{rs}(443)/R_{rs}(670)$	1.1578	−2.5984	1.6643	−0.4915	0.167
$R_{rs}(490)/R_{rs}(670)$	2.0115	−4.4879	3.3022	−1.0101	0.205
$R_{rs}(510)/R_{rs}(670)$	2.1981	−4.5871	3.2467	−1.1119	0.249

Table 3
Performance of empirical chlorophyll algorithms developed for data with bottom reflectance contributions at 555 nm less than 25% when applied to the entire data set ($n=451$) (all statistics calculated on log-transformed data)

Band-ratio	Slope	*y*-intercepts	r^2	$RMSE_{log10}$
$R_{rs}(412)/R_{rs}(555)$	1.044	0.107	0.69	0.302
$R_{rs}(443)/R_{rs}(555)$	1.015	0.078	0.78	0.251
$R_{rs}(490)/R_{rs}(555)$	1.011	0.058	0.80	0.233
$R_{rs}(510)/R_{rs}(555)$	1.081	0.085	0.74	0.277
$R_{rs}(412)/R_{rs}(670)$	1.006	−0.006	0.84	0.201
$R_{rs}(443)/R_{rs}(670)$	1.042	−0.011	0.83	0.216
$R_{rs}(490)/R_{rs}(670)$	1.314	0.058	0.59	0.434
$R_{rs}(510)/R_{rs}(670)$	1.566	0.122	0.41	0.627
Blend[a]	1.005	−0.005	0.88	0.172

[a] Data were classified as optically deep, optically shallow or transitional based on relationship between $R_{rs}(412)/R_{rs}(670)$ and $[R_{rs}(412)*R_{rs}(670)]/R_{rs}(555)^2$. Chlorophyll concentrations were derived using Chl_{deep} for optically deep data, $Chl_{shallow}$ for optically shallow data, and a weighted blend of these derived values for transitional data.

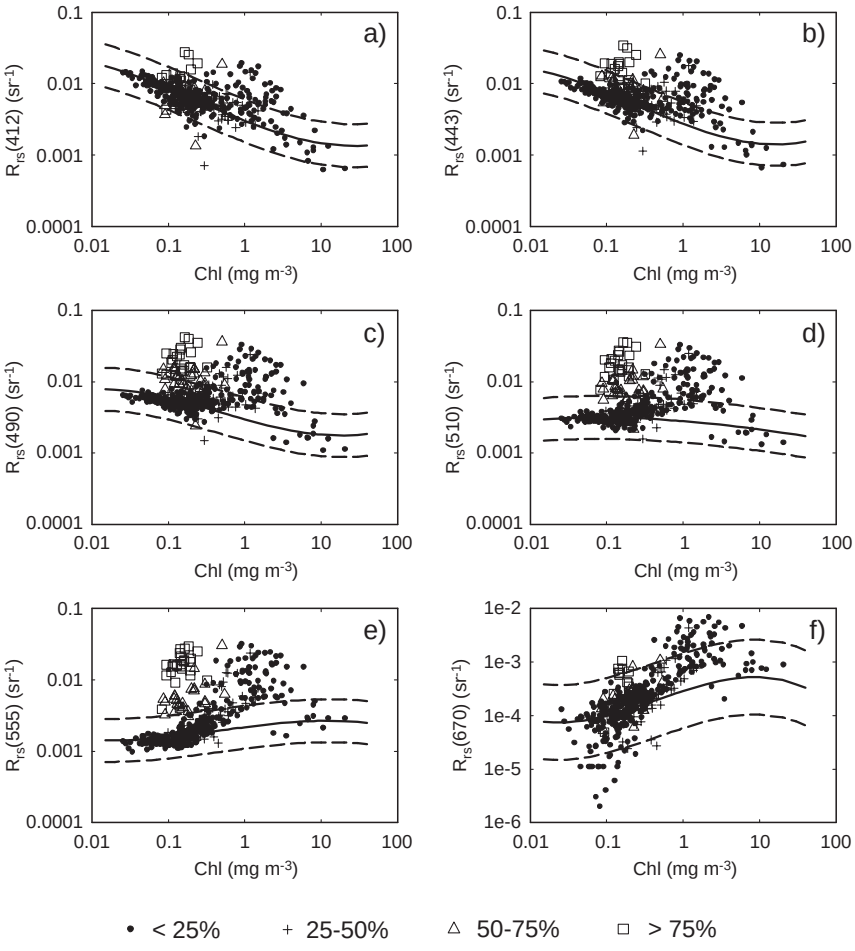

Fig. 6. Relationships between chlorophyll *a* concentrations and $R_{rs}(\lambda)$ where λ is (a) 412 nm, (b) 443 nm, (c) 490 nm, (d) 510 nm, (e) 555 nm and (f) 670 nm. Symbols are the same as in Fig. 5. Cubic polynomial functions derived for the SeaBAM data set (solid) (O'Reilly et al., 1998) are shown along with (a–e) 2:1 and 1:2 ratios and (f) 5:1 and 1:5 ratios of these functions (dashed).

the entire data set, the lowest error value for all the individual band-ratios examined was generated using $R_{rs}(412)/R_{rs}(670)$ ($RMSE_{log10}=0.201$) (Table 3). This value was 14% lower than the lowest error generated using the $R_{rs}(\lambda_1)/R_{rs}(555)$ best-fit cubic polynomial functions indicating that chlorophyll concentrations in optically shallow waters are more accurately derived using $R_{rs}(412)/R_{rs}(670)$ compared to using traditional blue-to-green band-ratios (e.g. $R_{rs}(490)/R_{rs}(555)$).

4.4. Development of classification and quantification techniques

While chlorophyll concentrations are estimated most accurately from $R_{rs}(412)/R_{rs}(670)$ for a data set containing 78% optically deep and 22% optically shallow data, concentrations for optically deep data only are estimated 24% less accurately from $R_{rs}(412)/R_{rs}(670)$ compared to $R_{rs}(490)/R_{rs}(555)$ (Table 2). One approach for optimizing algorithm performance in environments containing unknown bottom reflectance contributions is to first classify the data as optically deep or optically shallow. Chlorophyll concentrations can then be derived for optically deep data using the best-fit $R_{rs}(490)/R_{rs}(555)$ cubic polynomial function (or Chl_{deep}) and for optically shallow data using the best-fit $R_{rs}(412)/R_{rs}(670)$ cubic polynomial function (or $Chl_{shallow}$). In order to prevent switching artifacts from occurring (Müller-Karger et al., 1990), chlorophyll concentrations for so-called "transitional" data can be calculated from a blend of these derived values.

One of the greatest challenges for using such an approach is to be able to determine remotely whether a given data point or pixel is optically deep or optically shallow. One possible strategy for classifying data in terms of bottom reflectance contributions that is based on earlier observations and requires $R_{rs}(\lambda)$ data at only three wavebands (412, 555, and 670 nm) is introduced in Fig. 8. The band-ratio $R_{rs}(412)/R_{rs}(670)$ provides a surrogate for chlorophyll concentration with low ratios indicative of high concentrations and high ratios indicative of low concentrations (Fig. 7a). Recall that the majority of optically shallow data for this data set exhibit $R_{rs}(412)/R_{rs}(670)$ values greater than ~10 and chlorophyll concentrations less than ~0.5 mg m^{-3}. The spectral curvature about $R_{rs}(555)$, $[R_{rs}(412)*R_{rs}(670)]/R_{rs}(555)^2$ (or CURVE), provides an indicator of bottom reflectance contribution. Since $R_{rs}(412)$ and $R_{rs}(670)$ values are typically only mildly influenced by

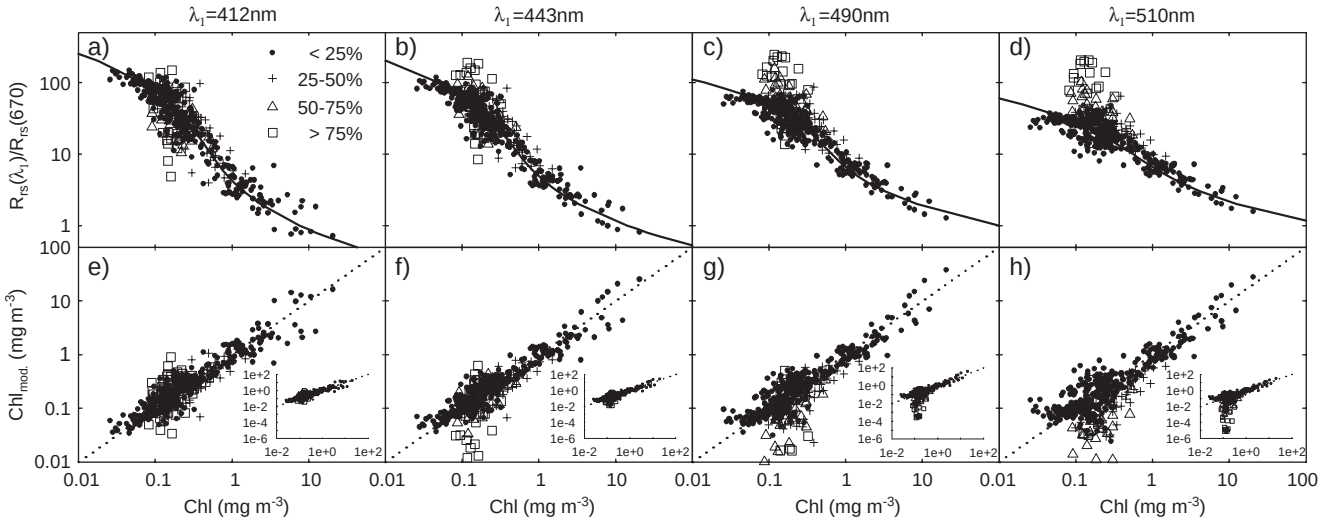

Fig. 7. Relationships between chlorophyll *a* concentrations and $R_{rs}(\lambda_1)/R_{rs}(670)$ (or R) where λ_1 is (a) 412 nm, (b) 443 nm, (c) 490 nm and (d) 510 nm. Symbols are the same as in Fig. 5. Cubic polynomial regression functions (solid) were fit to log-transformed optically deep (%bt_555<25%) data: $\log(\mathrm{Chl})=a_0+a_1\log(R)+a_2\log(R)^2+a_3\log(R)^3$. The best-fit cubic polynomial functions were applied to the entire data set and (e–h) measured versus modeled chlorophyll *a* concentrations and one-to-one lines (dotted) are shown.

bottom reflectance and $R_{rs}(555)$ values are highly perturbed by bottom reflectance (Fig. 6), CURVE values decrease as bottom reflectance contributions increase.

In order to classify the shipboard $R_{rs}(\lambda)$ data in this study as optically shallow, optically deep or transitional, the following classification criteria were developed (Fig. 8). A quadratic polynomial regression function was fit to the log-transformed optically deep data with %bt_555 values less than 25%: $\log(\mathrm{CURVE})=-1.22+0.40\log(R_{rs}(412)/R_{rs}(670))+0.04\log(R_{rs}(412)/R_{rs}(670))^2$. Dividing this best fit function by various factors (0.25, 0.5, 1, 1.5, 3, 6, and 12), parallel relationships were generated above and below the best-fit line to provide several possible combinations of so-called "upper" and "lower" threshold functions.

Data located above the upper threshold function and below the lower threshold function were classified as optically deep and optically shallow, respectively. Chlorophyll concentrations for these data were derived using Chl_{deep} and $\mathrm{Chl}_{shallow}$, respectively (Table 2). A weighting factor, w, equal to

$$w=\frac{\mathrm{CURVE}_{meas}-\mathrm{CURVE}_{lower}}{\mathrm{CURVE}_{upper}-\mathrm{CURVE}_{lower}} \quad (14)$$

was calculated for each transitional data point located between the upper and lower threshold functions where CURVE_{meas} is the measured curvature value, CURVE_{lower} is the curvature value calculated using the lower threshold function, and CURVE_{upper} is the curvature value calculated using the upper threshold function. Blended chlorophyll concentrations were then derived for transitional data as

$$\mathrm{Chl}=w\left(\mathrm{Chl}_{deep}\right)+(1-w)\left(\mathrm{Chl}_{shallow}\right). \quad (15)$$

All possible combinations of upper and lower threshold functions were tested until the lowest error value ($\mathrm{RMSE}_{log10}=0.172$) was attained (Fig. 9). This value was achieved using upper and lower threshold functions generated by dividing the best-fit quadratic polynomial function by the factors 0.5 and 6.0, respectively (Fig. 8).

The error value calculated using this new classification and quantification technique ($\mathrm{RMSE}_{log10}=0.172$) was 14% lower than the error value obtained when concentrations were determined using the best individual band-ratio, $R_{rs}(412)/R_{rs}(670)$. This error was 26% lower than the error calculated when concentrations were estimated using the traditional blue-to-green band-ratio, $R_{rs}(490)/R_{rs}(555)$, also employed by the O'Reilly et al. (1998) OC2 algorithm. Using this approach, overestimations in chlorophyll concentrations for optically shallow waters derived from $R_{rs}(490)/R_{rs}(555)$ and increased scatter for optically deep chlorophyll concentrations derived from $R_{rs}(412)/R_{rs}(670)$ that were previously observed (Figs. 5g and 7e) were reduced.

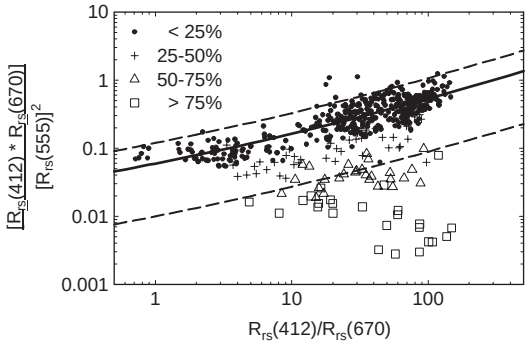

Fig. 8. Relationship between $R_{rs}(412)/R_{rs}(670)$ (or R) and $[R_{rs}(412)*R_{rs}(670)]/R_{rs}(555)^2$ (or CURVE). Symbols are the same as in Fig. 5. A quadratic polynomial regression function (solid) was fit to log-transformed optically deep (%bt_555<25%) data: $\log(\mathrm{CURVE})=-1.22+0.40\log(R)+0.04\log(R)^2$. The best-fit function was divided by 0.5 and 6.0 to generate the upper and lower threshold functions (dashed), respectively. Using these threshold functions, the lowest RMSE_{log10} value between measured and modeled chlorophyll *a* concentrations was calculated using the new blending technique.

5. Discussion

Empirical algorithms based on spectral band-ratios estimate chlorophyll *a* concentrations accurately and efficiently in most oceanic waters provided that phytoplankton dominate the optical properties and bottom reflectance is negligible (i.e. Case 1 waters) (Gordon et al., 1983; O'Reilly et al., 1998, 2000). For this reason, chlorophyll concentrations derived from satellite ocean color data collected by past (e.g. CZCS) and currently operational (e.g. SeaWiFS and MODIS) ocean color sensors are estimated using empirical algorithms. More complicated semi-analytic algorithms for deriving chlorophyll concentrations from coastal waters where non-biogenic optical properties (CDOM and detritus) do not co-vary with that of phytoplankton have also been developed (Carder et al., 1999). Both algorithm types, however, will overestimate chlorophyll concentrations in optically shallow waters if light reflected by the bottom is not removed prior to the algorithm being applied (Lee et al., 2001). While several inversion techniques (Lee et al., 1998a, 1998b, 1999) have been developed that are capable of retrieving bathymetry and bottom albedo from hyperspectral $R_{rs}(\lambda)$ data, water column optical properties including Chl are retrieved less accurately. Also, since these techniques perform optimally with hyperspectral data and can be computationally expensive (Lee et al., 1998a, 1998b), they are less suitable for routine application to large multi-spectral satellite scenes.

In this paper, a method is developed for quantifying chlorophyll concentrations more accurately in oceanic regions containing unknown bottom reflectance contributions. The method is computationally efficient and requires $R_{rs}(\lambda)$ data at only four wavebands (412, 490, 555, and 670 nm). These or similar wavebands are currently available for several operational satellite ocean color sensors (SeaWiFS, MODIS, and MERIS). Estimations of other inherent optical properties (e.g. $a_{ph}(\lambda)$, $a_{CDOM}(\lambda)$, and $b_{bp}(\lambda)$) may also be possible using the classification criteria developed in this study if empirical algorithms can be developed for these variables using wavebands less influenced by bottom reflectance.

Using this technique, data are first classified as optically shallow, optically deep, or transitional based on criteria developed for the relationship between the band-ratio $R_{rs}(412)/R_{rs}(670)$ and the spectral curvature about $R_{rs}(555)$, $[R_{rs}(412)*R_{rs}(670)]/R_{rs}(555)^2$. Chlorophyll concentrations for data classified as optically deep are calculated from $R_{rs}(490)/R_{rs}(555)$ using a cubic polynomial function developed in this study for data with bottom reflectance contributions at 555 nm less than 25%. An alternative empirical algorithm for data classified as optically shallow based on the band-ratio $R_{rs}(412)/R_{rs}(670)$ is developed from the %bt_555 less than 25% data. The logic behind using $R_{rs}(412)/R_{rs}(670)$ instead of $R_{rs}(490)/R_{rs}(555)$ for optically shallow waters is that $R_{rs}(412)$ and $R_{rs}(670)$ are typically located outside of the spectral transparency window and influenced less by bottom reflectance. Algorithm switching artifacts are avoided by using a weighted blend of chlorophyll concentrations derived by both band-ratio algorithms for data classified as transitional.

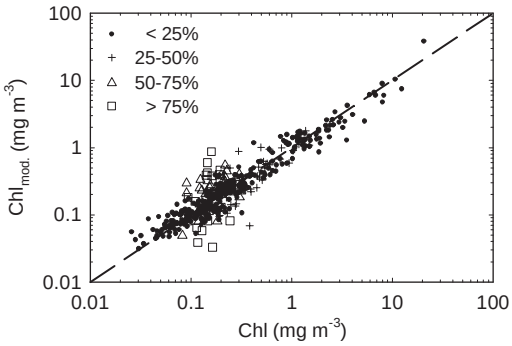

Fig. 9. Measured versus modeled chlorophyll *a* concentrations. Symbols are the same as in Fig. 5. Modeled concentrations were derived by classifying data as optically deep, optically shallow, or transitional based on the relationship between $R_{rs}(412)/R_{rs}(670)$ and $[R_{rs}(412)* R_{rs}(670)]/R_{rs}(555)2$. Chlorophyll concentrations were derived using Chldeep for optically deep data, Chlshallow for optically shallow data, and a weighted blend of these derived values for transitional data. A one-to-one line (dashed) is also shown.

While this technique may be applied immediately to shipboard and mooring data collected from the WFS and Bahamas, the success of this technique when applied to satellite-based ocean color data (e.g. SeaWiFS, MODIS) will rely on the radiometric accuracy of the sensor and proper atmospheric corrections of the imagery (McClain et al., 2000). Because corrections for aerosol reflectance are determined for infrared wavebands and then extrapolated using models to blue wavebands (Gordon & Wang, 1994), normalized water-leaving radiance values at 412 nm are more difficult to measure from space compared to radiance values at redder wavebands. Also, since pure water absorption is ~7 times higher at 670 nm compared to at 555 nm, $nL_w(670)$ values are difficult to measure due to the low signal-to-noise. Consequently, slight modifications to the classification criteria and empirical algorithms may be required when switching from shipboard to satellite $R_{rs}(\lambda)$ data.

The overall methodology developed in this paper may be applied to other oceanic regions besides the WFS and Bahamas that are influenced by bottom reflectance. However, the empirical algorithms and classification criteria may have to be adjusted regionally taking into account local $a_{CDOM}(\lambda)$ to $a_{ph}(\lambda)$ ratios. Due to the numerous rivers that outflow onto the WFS and the shallow nature of the shelf itself, CDOM-to-phytoplankton absorption ratios can exceed those observed for typical Case 1 waters and may differ for other regions. Since CDOM and phytoplankton both absorb blue light strongly, increases in blue-to-green absorption ratios due to increased CDOM result in decreases in blue-to-green reflectance ratios that can be mistaken for higher chlorophyll concentrations (Sathyendranath et al., 2001).

The multi-year, multi-season data set examined in this study was collected from many different oceanic environments on the WFS and from Bahamian waters. A wide range of chlorophyll concentrations (0.026 to 20.6 mg m^{-3}), bottom depths (3.6 to >1000 m), and bottom albedos ($0<\rho(550)_{mod.}<0.5$) were observed. Every possible combination of $a(\lambda)$, $b_b(\lambda)$, $\rho(\lambda)$ and H that naturally occurs, however, is not represented. Also, bottom types including seagrass and coral reefs,

vertically stratified water columns, and highly reflective coccolithophore (Balch et al., 1991) and *Trichodesmium* spp. (Subramaniam et al., 2002) blooms were not examined. Such conditions may not be classified or quantified accurately using this technique.

In order to determine the conditions under which the classification technique developed in this study may fail, a broad, robust library of synthetic $R_{rs}(\lambda)$ data generated for a wide range in chlorophyll concentrations, bottom depths and bottom albedos was examined (Carder et al., 2005). The results indicate that waters shallower than 5 m will be misclassified as optically deep using the classification criteria developed for the shipboard data in this study. Since reflectance data at 412 and 670 nm in such shallow waters are no longer outside the spectral transparency window, these data must be classified as optically shallow using additional criteria. Either a bathymetric flag or the addition of an absolute threshold criteria for $R_{rs}(555)$ above which waters are to be automatically classified as optically shallow are possibilities. It is very unlikely, however, that accurate chlorophyll concentrations can be retrieved from such shallow waters given that the water column reflectance signal is so low compared to the bottom reflectance signal.

Acknowledgements

Financial support was provided by NASA (NAS5-31716 and/or NNG04GL55G) and ONR (N00014-97-1-0006 and N00014-96-1-5013; or N00014-02-1-0211 and N00014-04-1-0531) funding. We thank David English, James Ivey, Daniel Otis, KePing Du, and Hari Warrior for their assistance in collecting and processing field data.

References

Antoine, D., Andre, J., & Morel, A. (1996). Oceanic primary production 2. Estimation at global scale from satellite (coastal zone color scanner) chlorophyll. *Global Biogeochemical Cycles*, *10*, 57–69.

Balch, W. M., Holligan, P. M., Ackleson, S. G., & Voss, K. J. (1991). Biological and optical properties of mesoscale coccolithophore blooms in the Gulf of Maine. *Limnology and Oceanography*, *36*, 629–643.

Bissett, W. P., Patch, J. S., Carder, K. L., & Lee, Z. P. (1997). Pigment packaging and Chl-*a* specific absorption in high-light oceanic waters. *Limnology and Oceanography*, *42*, 961–968.

Bricaud, A., Babin, M., & Morel, A. (1995). Variability in the chlorophyll-specific absorption coefficients of natural phytoplankton: Analysis and parameterization. *Journal of Geophysical Research*, *100*, 13321–13332.

Bricaud, A., & Stramski, D. (1990). Spectral absorption coefficients of living phytoplankton and nonalgal biogenous matter: A comparison between the Peru upwelling area and the Sargasso Sea. *Limnology and Oceanography*, *35*, 562–582.

Cannizzaro, J. P., Carder, K. L., Chen, F. R. Heil, C. A., Vargo, G. A. (in press). A novel technique for detection of the toxic dinoflagellate, *Karenia brevis*, in the Gulf of Mexico from remotely sensed ocean color data. *Continental Shelf Research*.

Carder, K. L., Cannizzaro, J. P., & Lee, Z. P. (2005). Ocean color algorithms in optically shallow waters: Limitations and improvements. In R. J. Frouin, M. Babin, & S. Sathyendranath (Eds.), *Proceedings of the Optics and Photonics Conference (vol. 5885)* Bellingham, WA: SPIE (San Diego, CA, 31 July 2005).

Carder, K. L., Chen, F. R., Lee, Z. P., Hawes, S. K., & Kamykowski, D. (1999). *Semi-analytic moderate-resolution imaging spectrometer algorithms for chlorophyll a and absorption with bio-optical domains based on nitrate-depletion temperatures*. *Journal of Geophysical Research*, *104*, 5403–5422.

Carder, K. L., Hawes, S. K., Baker, K. A., Smith, R. C., Steward R. G., et al. (1991). Reflectance model for quantifying chlorophyll *a* in the presence of productivity degradation products. *Journal of Geophysical Research*, *96*, 20599–20611.

Carder, K. L., Lee, Z. P., Chen, R. F., & Davis, C. O. (1993). Unmixing of spectral components affecting AVIRIS imagery of Tampa Bay. In G. Vane (Ed.), *Proc. SPIE 1937, Orlando, Florida* (pp. 77–90) .

Carder, K. L., Steward, R. G., Harvey, G. R., & Ortner, R. B. (1989). Marine humic and fulvic acids: Their effects on remote sensing of ocean chlorophyll. *Limnology and Oceanography*, *34*, 68–81.

Decho, A. W., Kawaguchi, K., Allison, M. A., Louchard, E. M., Reid, R. P., et al. (2003). Sediment properties influencing upwelling spectral reflectance signatures: The "biofilm gel effect". *Limnology and Oceanography*, *48*, 431–443.

D'Sa, E. J., Hu, C., Müller-Karger, F. E., & Carder, K. L. (2002). Estimation of colored dissolved organic matter and salinity fields in case 2 waters using SeaWiFS: Examples from Florida Bay and Florida Shelf. *Proceedings of the Indian Academy of Sciences. Earth and Planetary Sciences*, *111*, 197–207.

Eplee Jr., R. E., & McClain, C. R. (2000). SeaWiFS global clear-water analysis. *Volume 10, SeaWiFS Postlaunch Calibration and Validation Analyses, Part 2, NASA Tech. Memo. 2000-206892, Vol. 10* Greenbelt, MD: NASA Goddard Space Flight Center.

Gordon, H. R., Brown, O. B., Evans, R. H., Brown, J. W., Smith, R. C., et al. (1988). A semianalytic radiance model of ocean color. *Journal of Geophysical Research*, *93*, 10909–10924.

Gordon, H. R., Clark, D. K., Brown, J. W., Brown, O. B., Evans, R. H., et al. (1983). Phytoplankton pigment concentrations in the Middle Atlantic Bight: Comparison of ship determinations and CZCS estimates. *Applied Optics*, *22*, 20–36.

Gordon, H. R., & Wang, M. (1994). Retrieval of water-leaving radiance and aerosol optical thickness over the oceans with SeaWiFS: A preliminary algorithm. *Applied Optics*, *33*, 443–452.

Gould Jr., R. W., & Arnone, R. A. (1997). Remote sensing estimates of inherent optical properties in a coastal environment. *Remote Sensing of Environment*, *61*, 290–301.

Gregg, W. W., & Conkright, M. E. (2002). Decadal changes in global ocean chlorophyll. *Geophysical Research Letters*, *29*, 1730.

Holm-Hansen, O., & Riemann, B. (1978). Chlorophyll *a* determination: Improvements in methodology. *Oikos*, *30*, 438–447.

Hu, C., Müller-Karger, F., Carder, K. L., & Lee, Z. (1998). A method to derive optical properties over shallow waters using SeaWiFS. In S. Ackleson, & J. Campbell (Eds.), *Ocean Optics XIV Conference* (pp. 1–8) (Kailua-Kona, HI, 10–13 November 1998 (CD-ROM)).

Kiefer, D. A., & SooHoo, J. B. (1982). *Spectral absorption by marine particles of coastal waters of Baja California*. *Limnology and Oceanography*, *27*, 492–499.

Kishino, M., Takahashi, M., Okami, N., & Ichimura, S. (1985). Estimation of the spectral absorption coefficients of phytoplankton in the sea. *Bulletin of Marine Science*, *37*, 634–642.

Lee, Z. (1994). Visible-infrared remote-sensing model and applications for oceanic waters, PhD dissertation, University of South Florida, St. Petersburg, FL.

Lee, Z., & Carder, K. L. (2002). Effect of spectral band numbers on the retrieval of water column and bottom properties from ocean color data. *Applied Optics*, *41*, 2191–2201.

Lee, Z., Carder, K. L., Chen, R. F., & Peacock, T. G. (2001). Properties of the water column and bottom derived from Airborne Visible Infrared Imaging Spectrometer (AVIRIS) data. *Journal of Geophysical Research*, *106*, 11639–11651.

Lee, Z., Carder, K. L., & Du, K. (2004). Effects of molecular and particle scatterings on the model parameter for remote-sensing reflectance. *Applied Optics*, *43*, 4957–4964.

Lee, Z., Carder, K. L., Mobley, C., Steward, R. G., & Patch, J. S. (1998). Hyperspectral remote sensing for shallow waters: I. A semi-analytical model. *Applied Optics*, *37*, 6329–6338.

Lee, Z., Carder, K. L., Mobley, C. D., Steward, R. G., & Patch, J. S. (1999). Hyperspectral remote sensing for shallow waters: 2. Deriving bottom depths and water properties by optimization. *Applied Optics*, *38*, 3831–3843.

Lee, Z., Carder, K. L., Steward, R. G., Peacock, T. G., Davis, C. O., et al. (1997). Remote-sensing reflectance and inherent optical properties of oceanic waters derived from above-water measurements. In S. G. Ackleson, & R. Frouin (Eds.), *Proceedings of the Ocean Optics XIII Conference*, *vol. 2963* (pp. 1960–1966) (Bellingham, WA: SPIE. Halifax, Nova Scotia, 1996).

Lee, Z. P., Zhang, M. R., Carder, K. L., & Hall, L. O. (1998). *A neural network approach to deriving optical properties and depths of shallow waters*. In S. Ackleson, & J. Campbell (Eds.), *Ocean Optics XIV Conference* (pp. 1–7) (Kailua-Kona, HI, 10–13 November 1998 (CD-ROM)).

Louchard, E. M., Reid, R. P., Stephens, F. C., Davis, C. O., Leathers, R. A., et al. (2003). *Optical remote sensing of benthic habitats and bathymetry in coastal environments at Lee Stocking Island, Bahamas: A comparative spectral classification approach*. *Limnology and Oceanography*, *48*, 511–521.

Lyzenga, D. R. (1978). Passive remote sensing techniques for mapping water depth and bottom features. *Applied Optics*, *17*, 379–383.

Maffione, R. A., & Dana, D. R. (1997). Instruments and methods for measuring the backward-scattering coefficient of ocean waters. *Applied Optics*, *36*, 6057–6067.

Maritorena, S., Morel, A., & Gentili, B. (1994). Diffuse reflectance of oceanic shallow waters: Influence of water depth and bottom albedo. *Limnology and Oceanography*, *39*, 1689–1703.

McClain, C. R., Barnes, R. A., Eplee Jr., R. E., Franz, B. A., Hsu, N. C. et al. (2000). SeaWiFS postlaunch calibration and validation analyses. Part 2. *NASA Tech. Memo. 2000-206892, vol. 10.* (pp. 1–24) London: NASA Goddard Space Flight Center.

Mobley, C. D., Sundman, L. K., Davis, C. O., Bowles, J. H., Downes, T. V., et al. (2005). Interpretation of hyperspectral remote-sensing imagery via spectrum matching and look-up tables. *Applied Optics*, *44*, 3576–3592.

Morel, A. (1974). Optical properties of pure water and pure sea water. In N. G. Jerlov, & E. S. Nielsen (Eds.), *Optical aspects of oceanography* (pp. 1–24) London: Academic Press.

Morel, A., & Gentili, B. (1993). Diffuse reflectance of oceanic waters: Part 2. Bidirectional aspects. *Applied Optics*, *32*, 6864–6879.

Mueller, J. L. & Fargion, G. S. (2002). Ocean optics protocols for satellite ocean color sensor validation, revision 3, volume 2. *NASA Tech. Memo. 2002-210004/Rev3-Vol2*, NASA Goddard Space Flight Center, Greenbelt, MD.

Müller-Karger, F. E., McClain, C. R., Sambrotto, R. N., & Ray, G. C. (1990). A comparison of ship and coastal zone color scanner mapped distribution of phytoplankton in the southeastern Bering Sea. *Journal of Geophysical Research*, *95*, 11483–11499.

Nelson, J. R., & Robertson, C. Y. (1993). Detrital spectral absorption: Laboratory studies of visible light effects on phytodetritus absorption, bacterial spectral signal, and comparison to field measurements. *Journal of Marine Research*, *51*, 181–207.

O'Reilly, J. E., Maritorena, S., Mitchell, B. G., Siegel, D. A., Carder, K. L., et al. (1998). Ocean color chlorophyll algorithms for SeaWiFS. *Journal of Geophysical Research*, *103*, 24937–24953.

O'Reilly, J. E., Maritorena, S., Siegel, D. A., O'Brien, M. C., Toole, D., et al. (2000). Ocean color chlorophyll a algorithms for SeaWiFS, OC2, and OC4: Version 4. *SeaWiFS postlaunch calibration and validation analyses, Part 3, NASA Tech. Memo. 2000-206892, vol. 11* Greenbelt, MD: NASA Goddard Space Flight Center.

Pope, R., & Fry, E. (1997). Absorption spectrum (380–700 nm) of pure waters: II. Integrating cavity measurements. *Applied Optics*, *36*, 8710–8723.

Roesler, C. S., Perry, M. J., & Carder, K. L. (1989). Modeling in situ phytoplankton absorption from total absorption spectra in productive inland marine waters. *Limnology and Oceanography*, *34*, 1510–1523.

Sandidge, J. C., & Holyer, R. J. (1998). Coastal bathymetry from hyperspectral observations of water radiance. *Remote Sensing of Environment*, *65*, 341–352.

Sathyendranath, S., Cota, G., Stuart, V., Maass, H., & Platt, T. (2001). Remote sensing of phytoplankton pigments: A comparison of empirical and theoretical approaches. *International Journal of Remote Sensing*, *22*, 249–273.

Spitzer, D., & Dirks, R. W. J. (1987). Bottom influence on the reflectance of the sea. *International Journal of Remote Sensing*, *8*, 279–290.

Subramaniam, A., Brown, C. W., Hood, R. R., Carpenter, E. J., & Capone, D. G. (2002). Detecting Trichodesmium blooms in SeaWiFS imagery. *Deep-Sea Research. II*, *49*, 107–121.

Trees, C. C., Clark, D. K., Bidigare, R. R., Ondrusek, M. E., & Mueller, J. L. (2000). Accessory pigments versus chlorophyll *a* concentrations within the euphotic zone: A ubiquitous relationship. *Limnology and Oceanography*, *45*, 1130–1143.

Werdell, P. J., & Roesler, C. S. (2003). Remote assessment of benthic substrate composition in shallow waters using multispectral reflectance. *Limnology and Oceanography*, *48*, 557–567.

Yentsch, C. S. (1962). Measurement of visible light absorption by particulate matter in the ocean. *Limnology and Oceanography*, *7*, 207–217.